Taylor & Francis
Taylor & Francis Group

Phosphorus, Sulfur, and Silicon and the Related Elements

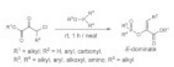

ISSN: 1042-6507 (Print) 1563-5325 (Online) Journal homepage: www.tandfonline.com/journals/gpss20

Synthesis and characterization of acrylic acid-based SiO_2 nanocomposite hydrogels

Fatma Özge Gökmen & Nursel Pekel Bayramgil

To cite this article: Fatma Özge Gökmen & Nursel Pekel Bayramgil (2023) Synthesis and characterization of acrylic acid-based SiO_2 nanocomposite hydrogels, Phosphorus, Sulfur, and Silicon and the Related Elements, 198:1, 63-71, DOI: 10.1080/10426507.2022.2113979

To link to this article: https://doi.org/10.1080/10426507.2022.2113979

Published online: 10 Sep 2022.

PHOSPHORUS, SULFUR, AND SILICON AND THE RELATED ELEMENTS
2023, VOL. 198, NO. 1, 63–71
https://doi.org/10.1080/10426507.2022.2113979

Synthesis and characterization of acrylic acid-based SiO_2 nanocomposite hydrogels

Fatma Özge Gökmen[a,b] and Nursel Pekel Bayramgil[a]

[a]Faculty of Science, Chemistry Department, Hacettepe University, Ankara, Turkey; [b]Central Research Laboratory, Bilecik Şeyh Edebali University, Bilecik, Turkey

ABSTRACT

Acrylic acid (AA) nanocomposite hydrogels (NCH) containing different kinds of SiO_2 nanoparticles were prepared by way of free radical polymerization. The polymerization conditions were optimized considering the initiator and monomer concentrations in the mixture, as well as the reaction temperature and time. SiO_2 nanoparticles were used in original (neutral), NH_2 modified (hydrophilic) and perlite forms. Nanocomposite hydrogels that contain NH_2 modified nano-SiO_2 were found to present swelling values higher than those of the original acrylic acid nanocomposite hydrogel and the nanocomposite hydrogel that contain original SiO_2. AA-perlite nanocomposite hydrogels were used to achieve the best thermal stability, although the perlite-doped hydrogels exhibit less swelling due to the large particle size of perlite and its lower SiO_2 content. FESEM and mapping analyses were conducted to verify the incorporation of SiO_2 nanoparticles into the hydrogel structure. Amorphous structures were determined by an XRD analysis. Thermal stability of hydrogels was measured by TG-DTA. The thermal stabilities of NH_2-modified SiO_2- and perlite-doped nanocomposite hydrogels were found to be higher than those of plain hydrogel and original SiO_2-doped nanocomposite hydrogels.

ARTICLE HISTORY
Received 28 June 2022
Accepted 13 August 2022

KEYWORDS
Nanocomposite hydrogels; nano-SiO_2; SEM-mapping; acrylic acid

GRAPHICAL ABSTRACT

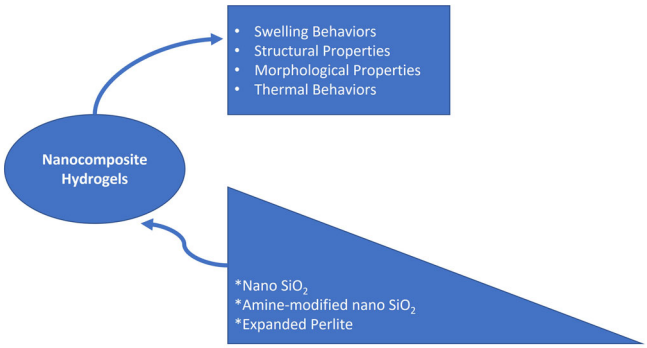

Introduction

As they can mimic the chemical, physical, electrical, and biological properties of most biological tissues, hydrogels are one of the potential candidates among other biomaterials.[1–3] They have a highly hydrated, three-dimensional (3-D) polymeric network and are capable of holding up to 20- to 40-fold more water in comparison to their dry weight. These networks can be shaped or cast into different sizes and shapes thanks to their unique physical properties.[4]

Hydrogels have drawn tremendous interest in the field of biomedicine since the discovery of poly(2-hydroxyethyl methacrylate) by Wichterle and Lim in 1960.[5] Currently, hydrogels are being investigated for their potential as a delivery system for bioactive molecules thanks to their similar physical properties with those of living tissues, which is associated with their soft and rubbery consistency, high water content, as well as low interfacial tension with water or biological fluids. Anionic hydrogels are employed in designing intelligent controlled release devices for site-specific drug delivery of therapeutic proteins to the large intestine, which is characterized by a prolonged biological activity of the proteins. On the other hand, cationic hydrogels are investigated to develop a self-regulated insulin delivery system to release insulin in response to changes in glucose concentration.[6]

In recent years, interest in nanocomposite hydrogels for use in various biomedical applications has increased. Improved surface interactions between nanoparticles and

CONTACT Nursel Pekel Bayramgil nursel@hacettepe.edu.tr, nurselbayramgil@gmail.com Faculty of Science, Chemistry Department, Hacettepe University, 06800 Ankara, Turkey.

Table 1. Conversion, gelation and swelling properties of nanocomposite hydrogels.

Plain AA			Neutral nano-SiO_2-doped AA			Amine-modified nano-SiO_2-doped AA			EP-doped AA		
C%	G%	S%	C%	G%	S%	C%	G%	S%	C%	G%	S%
90 ± 0.82	99 ± 0.82	350 ± 1.25	99 ± 0.82	99 ± 0.82	360 ± 1.25	97 ± 1.25	99 ± 0.82	320 ± 1.25	95 ± 1.25	97 ± 1.25	340 ± 1.25

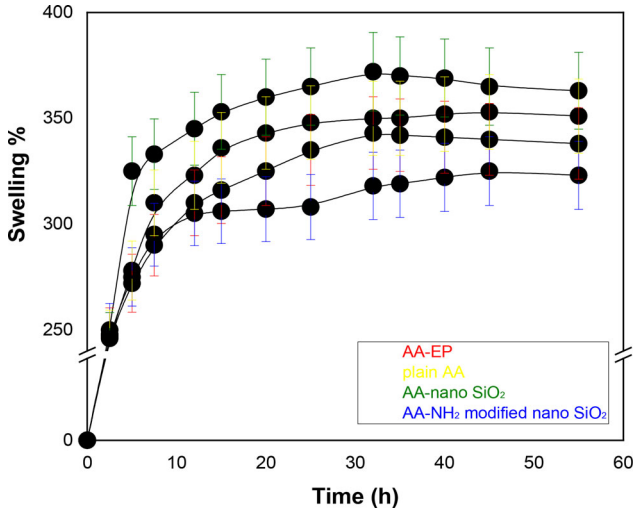

Figure 1. Swelling ratio of AA, AA/EP, AA/nano-SiO_2, AA/*hf* nano-SiO_2 hydrogels.

polymer chains provide material properties that could prove to be useful for a variety of biomedical applications. However, the majority of current nanocomposite techniques lack control over key characteristics including stimulus response and biodegradation. Alternative methodologies for designing nanocomposite hydrogels with diverse functions have been proposed to solve these issues.[4]

Several properties can be integrated by combining several phases inside a nanocomposite hydrogel network to replicate the structure and behavior of real tissues. For example, inorganic nanoplatelets (ceramic nanoparticles) can physically interact with aliphatic ester dendrimers coupled with the PEG spacer to generate physically crosslinked hydrogels.[7] The crosslinked networks feature self-healing qualities, great mechanical strength, and adhesive properties, which is interesting. This shows how a multicomponent system can be used to achieve diverse functionality inside a hybrid hydrogel network. In some studies, hydrogels meet the requirements for use as matrix (carriers) in controlled drug delivery, especially electroactive ones. It has been proven that the most basic requirement is that the matrix on which drugs are supported is sensitive to drug dosage against internal and/or external stimuli of different structures such as pressure, pH, temperature, ionic strength or electricity.[8]

Researchers have been designing the next generation of sophisticated biomaterials by mixing inorganic ceramic nanoparticles with natural or synthetic polymers, which are inspired by bioactive nanomaterials found in biological tissues. Bioactive nanoparticles such as hydroxyapatite (nHA), synthetic silicate nanoparticles, bioactive glasses, silica, calcium phosphate, glass ceramic, and β-wollastonite have been described for biological uses in recent decades.[9]

For the synthesis of hydrogels, several approaches have been documented. The first method uses a multifunctional monomer as a crosslinking agent to polymerize/crosslink monomers. The polymerization process begins chemically. This reaction might take place in bulk, solution, or suspension form. Irradiation or chemical substances are used to crosslink linear polymers in the second approach.[10–14]

Thakur et. al.[15] reported the fabrication of SA-*g*-PAA/TiO_2 and SA-*g*-PAA nanocomposite by a free radical graft copolymerization method to use the nanocomposite hydrogels, which presented a high adsorption capacity as an adsorbent, removing methylene blue from water. Makhado et. al.[16] reported a graft copolymerization of acrylic acid (AA) onto xanthan gum (XG), inducted by the method of microwave radiation, to determine the kinetic model of removing dye from wastewater.

The use of silica nanoparticles in drug delivery systems is increasingly being investigated. Although there are many reasons, the main reason is that the cytotoxicity of silica nanoparticles has been discovered to be closely linked to many factors such as their size, dose, cell type in the study, duration of treatment, surface area and structural separation.[17] In recent years, silica nanoparticles have been developed for use in versatile drug delivery systems due to their inherent properties such as stability, tunable porosity, mesoporous nature, biocompatibility, ease of functionalization, and non-degradation. Moreover, the chemical modification technique is suitable for obtaining targeted internalization, stimuli-responsive release, increased circulation time, and contrast imaging agents.[18]

In the present study, nanocomposite hydrogels based on acrylic acid (AA) including different kinds of SiO_2 nanoparticles (as reinforcing agents) were prepared by way of free radical polymerization. Their physical, structural, morphological and thermal properties were investigated in order to assess their applicability to controlled drug delivery systems.

Results and discussion

In the present study, the acrylic acid nanocomposite hydrogels were obtained with three kinds of SiO_2 by way of free radical polymerization. Percentage conversion (C%), gel percentage (G%) and swelling percentage (S%) of nanocomposite hydrogels are presented in Table 1. As can be seen from the table, while the C% obtained for pure AA hydrogel was 90, C% values higher than 95 were achieved for the nanocomposite hydrogels that were obtained with the inclusion of SiO_2 nanoparticles. This increase could likely be explained by the fact that the H-bonds formed between –OH groups, found abundantly in the SiO_2 structure, and the –COOH groups of acrylic acid facilitate polymerization. The G% for all hydrogels were found to be 99 except the EP-doped AA nanocomposite hydrogels. Compared with others, the lower value found here could also be associated with EP's particle size, which is larger. Figure 1 shows the S%-time curves for plain AA hydrogel and its nanocomposites.

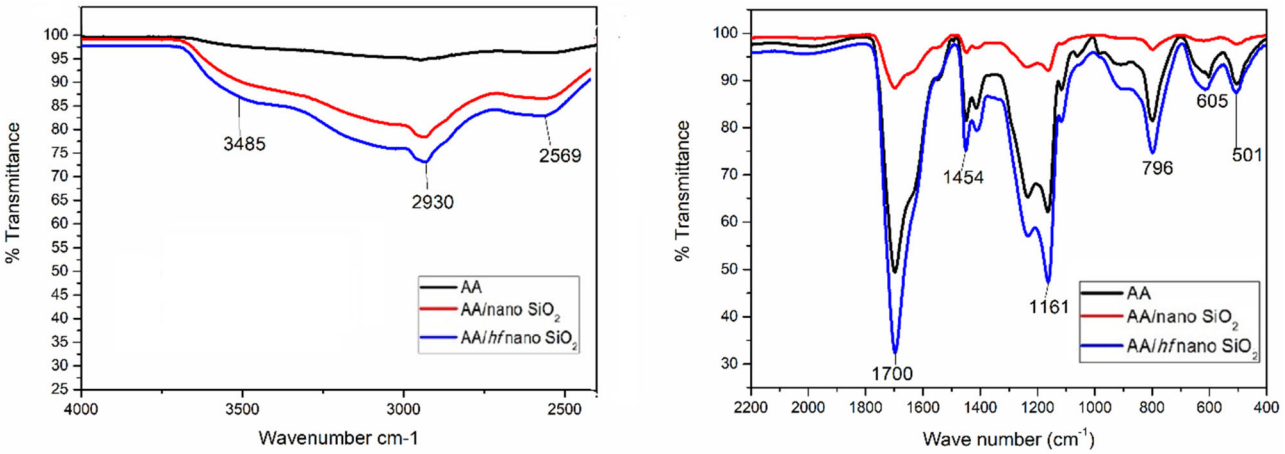

Figure 2. FT-IR spectra of AA, AA/nano SiO_2 and AA/*hf* nano SiO_2 hydrogels.

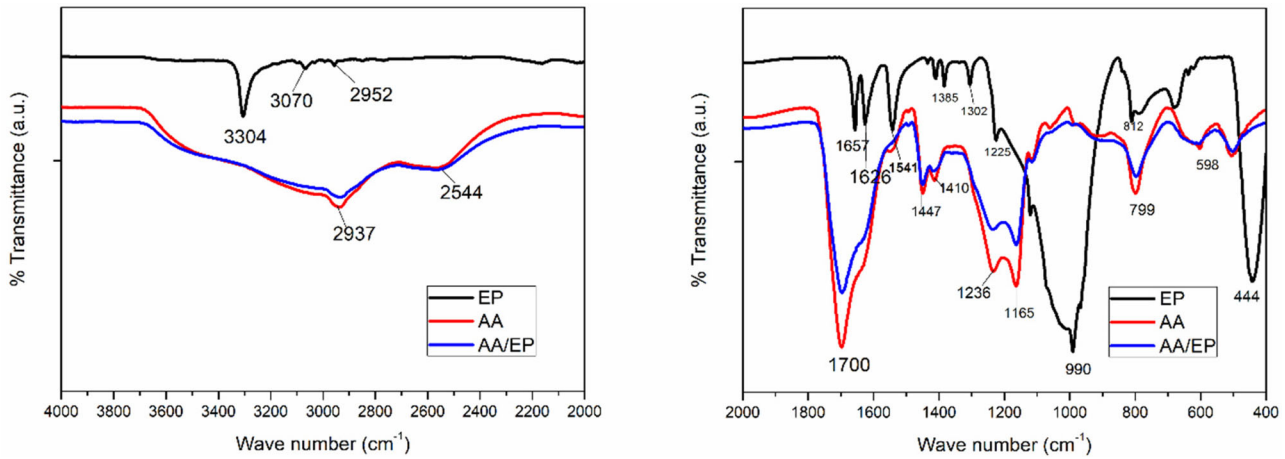

Figure 3. FT-IR spectra of AA and AA/EP hydrogels.

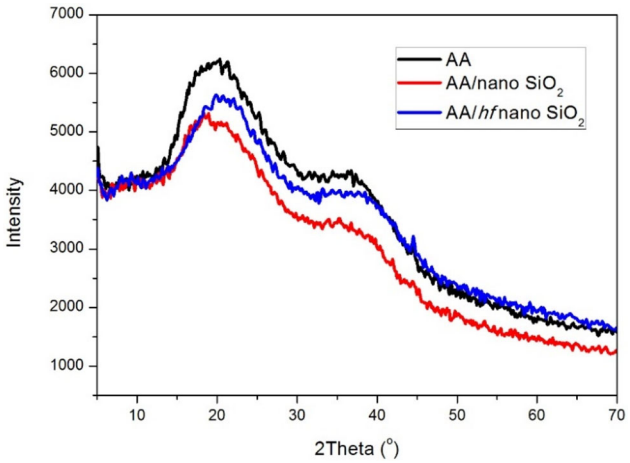

Figure 4. XRD patterns of AA, AA/nano SiO_2 and AA/*hf* nano SiO_2 hydrogels.

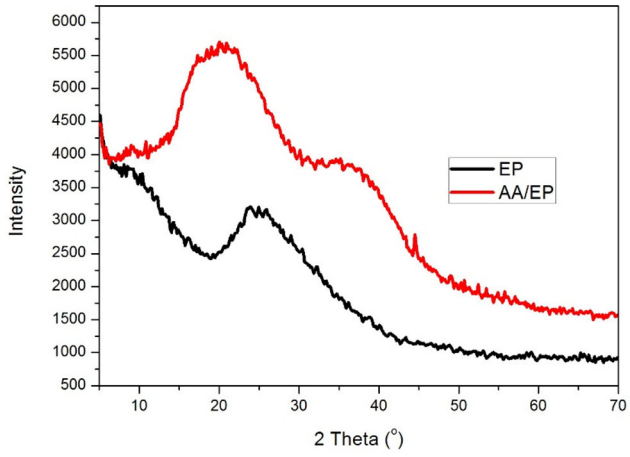

Figure 5. XRD patterns of EP and AA/EP hydrogel.

S% values of nanocomposite hydrogels, except for neutral SiO_2-doped AA nanocomposite hydrogels, were lower than plain AA hydrogels. In polyacrylic acid, regularly repeated and crosslinked acrylic acid units shift to an irregular structure with the addition of inorganic material, and the structure itself partly loses cohesion as well. Therefore, the interaction of water with the acrylic acid groups by diffusing into the hydrogel is prevented by SiO_2 nanoparticles. This is why swelling rates are found to be low. However, the case is different with neutral SiO_2 nanoparticles. The –OH groups (in neutral SiO_2), which are abundant within the structure, also have a capacity of interaction with water. For this reason, albeit not much, it may have slightly increased the swelling effect.[19] The reason for this can be explained as the fact that the porous structure of the hydrogel was filled with H_2O-bound SiO_2 nanoparticles which lead to enlargement of

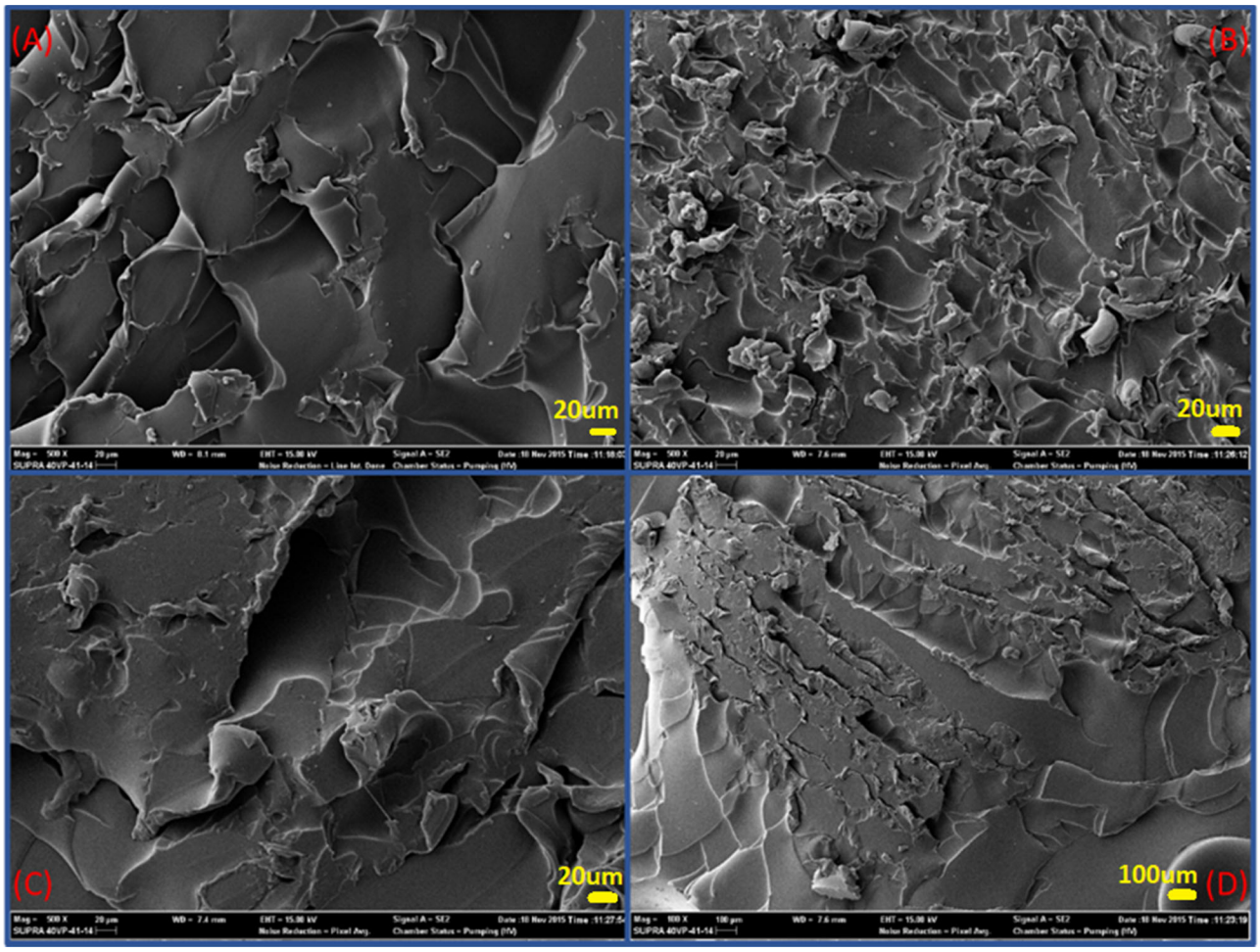

Figure 6. FESEM images of (A) plain AA hydrogel; (B) nano SiO_2 doped AA hydrogel; (C) amine-modified nano SiO_2 doped AA hydrogel and (D) EP doped AA hydrogel.

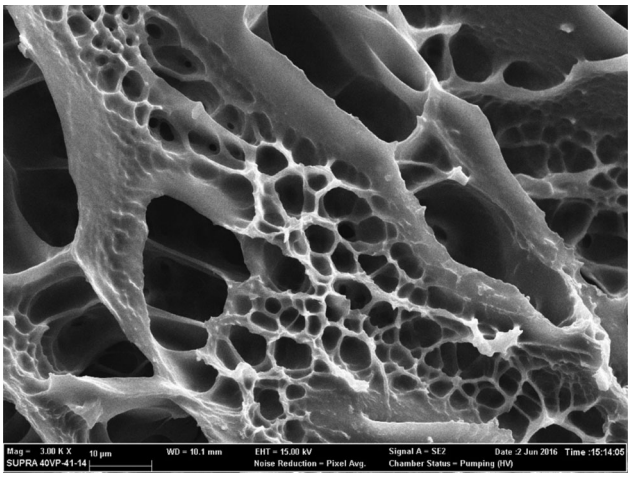

Figure 7. FESEM image of lyophilized AA hydrogel (3000x).

hydrogel's structure. Upon a visual evaluation of the hydrogel's dimensional stability, the best reinforcement-matrix compatibility was observed in the NH_2-modified nano-SiO_2-added nanocomposite hydrogel, despite it's the lowest swelling rate. Due to a possible H-bond between acrylic acid groups and NH_2 groups, the interaction of water with a less acrylic acid group may account for the lower swelling rate compared with that of others. In the later parts of the study, perlite was chosen based on its affordability.

Perlite was used in its expanded form because of its high surface area. The trace elements in the expanded perlite also caused the possible interaction with the matrix to be lower, leading to a slightly decreased swelling rate.[20]

Although the swelling value is lower than the others, NH_2-modified SiO_2 nanoparticles have two important advantages in this study: First, SiO_2 nanoparticles can be homogeneously dispersed into the AA matrix due to possible interactions between the NH_2 groups and the -COOH groups of acrylic acid. Secondly, the presence of NH_2 groups in addition to the -COOH groups increases the adsorption ability of the nanocomposite hydrogel. The validity of this statement was demonstrated by the results obtained in another study and our study was sent for publication.

The structures of pure AA and its nanocomposite hydrogels were illuminated using the FT-IR method. When the FT-IR spectra of the original AA and nano SiO_2-doped AA nanocomposite hydrogels were examined, shown in Figure 2, the bands at 1710 cm^{-1} ($\nu_{C=O}$) and 1560 cm^{-1} ($\nu_{asymC=O}$) are characteristics of acrylic acid units. Additionally, the ν_{CH} and ν_{CH2} vibrations were observed at 2944 cm^{-1} and 2860 cm^{-1}, and δ_{OH} vibrations of adsorbed water at 3150 cm^{-1}. It is noteworthy after the addition of nano SiO_2

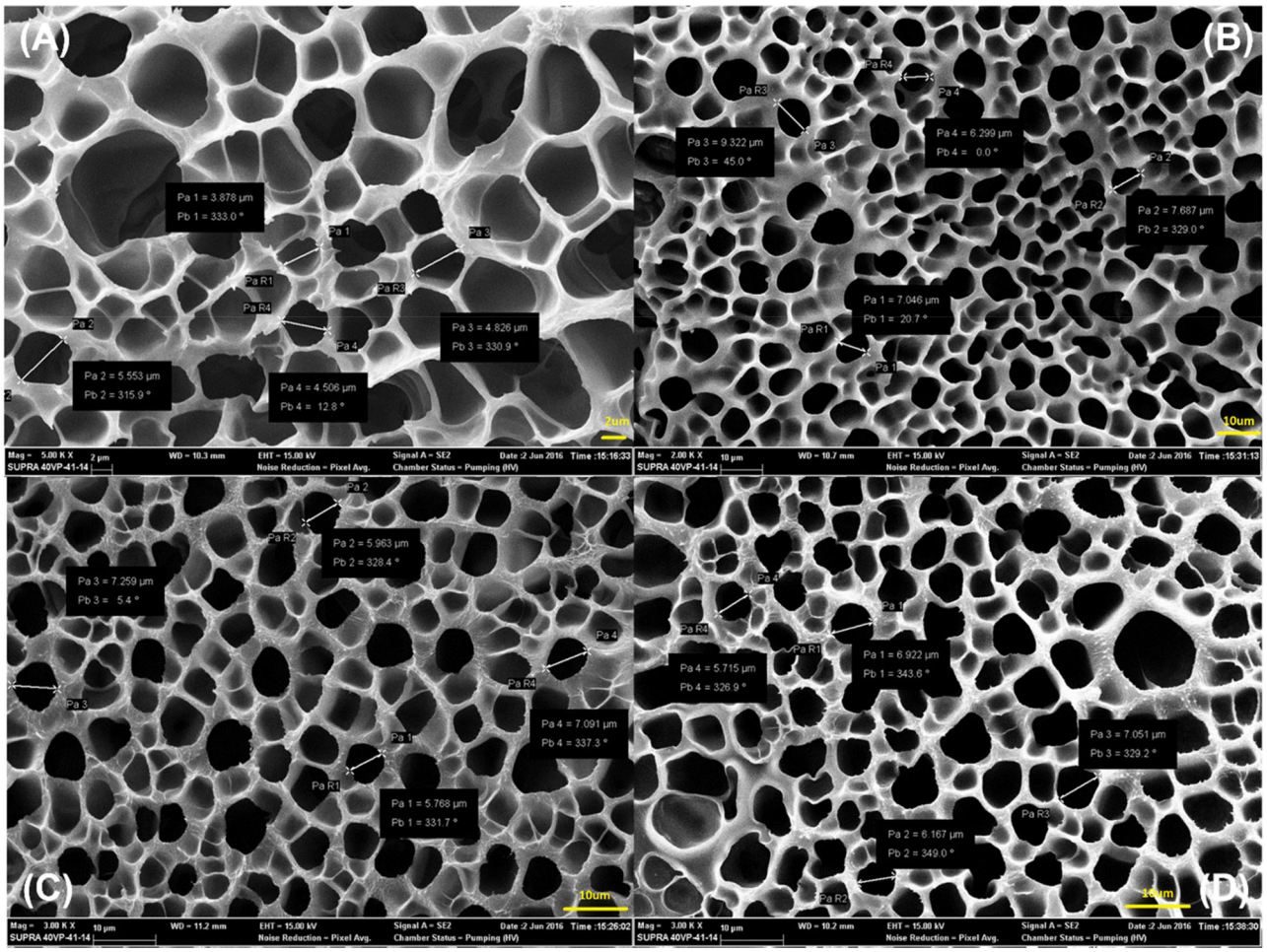

Figure 8. FESEM images of lyophilized (A) plain AA hydrogel; (B) nano SiO_2 doped AA hydrogel; (C) amine modified nano SiO_2 doped AA hydrogel; (D) EP doped AA hydrogel.

Table 2. Average pore size of AA hydrogel and SiO_2-based nanocomposite hydrogels.

	Plain AA	Neutral nano-SiO_2 doped AA	Amine-modified nano-SiO_2 doped AA	EP-doped AA
Pore size (μm)	4.691	7.588	8.694	6.464

into AA, ν_{CH} vibrations were apparent and the intensity of δ_{OH} vibrations of adsorbed water increased at 3150 cm^{-1}. The vibrations at 850 cm^{-1} ($\nu_{Si\text{-}O\text{-}Si}$) and 470 cm^{-1} ($\delta_{Si\text{-}O\text{-}Si}$) are also the most important evidence that nano SiO_2 is incorporated into the AA structure.[21] On the other hand, the sharpening of the $\nu_{C=O}$ vibrations at 1710 cm^{-1}, ν_{NH} vibrations at 3500 cm^{-1} and δ_{NH} vibrations at 1560 cm^{-1} are attributed to the NH_2 groups of *hf* nano SiO_2 particles added to the AA structure.[21] Compared with 3 kinds of reinforcement materials on the AA matrix, the best structural harmony was seen between AA and *hf* nano-SiO_2. The strong interaction between the reinforcement and matrix is clearly shown in Figure 2. H-bonds firmly increased the peak intensities at 1710 cm^{-1} and 3150 cm^{-1}.

When the FT-IR spectrum of the EP-doped AA nanocomposite hydrogel was examined, which is presented in Figure 3, the most significant change is the vibrations at 3150 cm^{-1} (δ_{OH}). Moreover, while the source of the vibrations at 850 cm^{-1} was $\nu_{Si\text{-}O\text{-}Si}$, the $\nu_{Si\text{-}O\text{-}Si}$ vibrations in the heat-treated EP were also observed at 1010 cm^{-1}.[22]

Figure 4 shows the XRD patterns of the AA nanocomposite hydrogels and pure AA hydrogel. The structure of acrylic acid is naturally amorphous. It has been observed in the literature that AA gives an intensity of 100% peak at 23.5°.[23] At the 2Theta (2θ) 23.5° peak found in the literature, acrylic acid was shifted to 19.5° when synthesized in the hydrogel form. Nano SiO_2-added hydrogels caused an increased intensity at XRD peaks and also increased at full-width at half-maximum (FWHM).

The effect of EP on AA hydrogel is presented in the XRD patterns given in Figure 5. The angle of AA at $2\theta = 23.5°$ shifted to the lower region as a result of the addition of EP to the hydrogel structure. These shifts presented in both XRD patterns may also be due to the presence of water and cross-linked regions included in hydrogel structure.[22]

Morphological characterization of AA and nanocomposite hydrogels was achieved by SEM. Figure 6 shows the FESEM images of the AA and its nanocomposite hydrogels. The surface of AA hydrogel was not smooth before the lyophilization process (Figure 6A). The nanocomposite hydrogel, which has the lowest surface roughness, is the AA nanocomposite hydrogel obtained by adding *hf* nano SiO_2, as explained just before (Figure 6C).

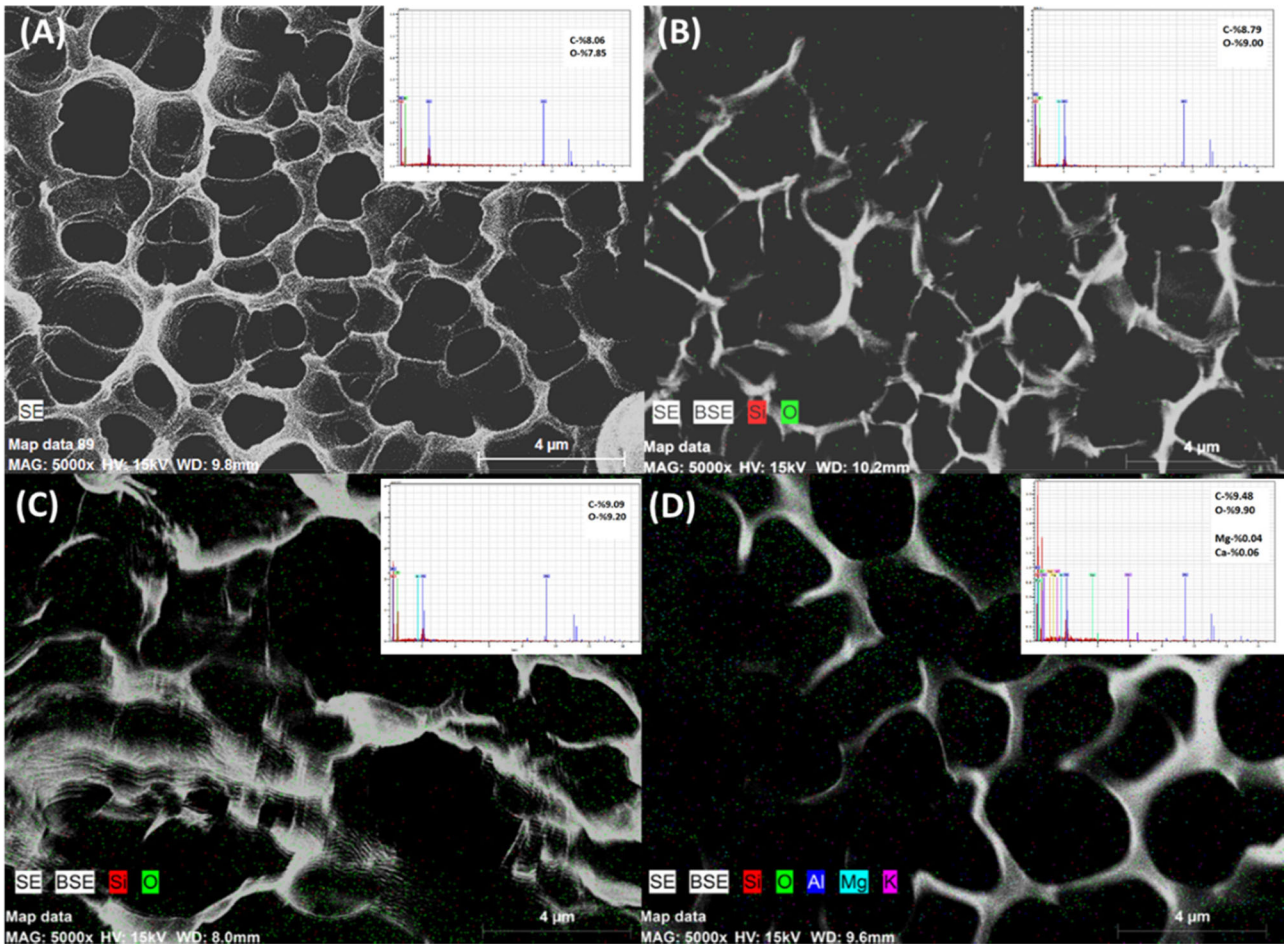

Figure 9. Mapped images and EDX spectra of lyophilized AA (A); (B): AA/nano SiO_2; (C): AA/amine-modified nano SiO_2; (D): AA/EP hydrogels.

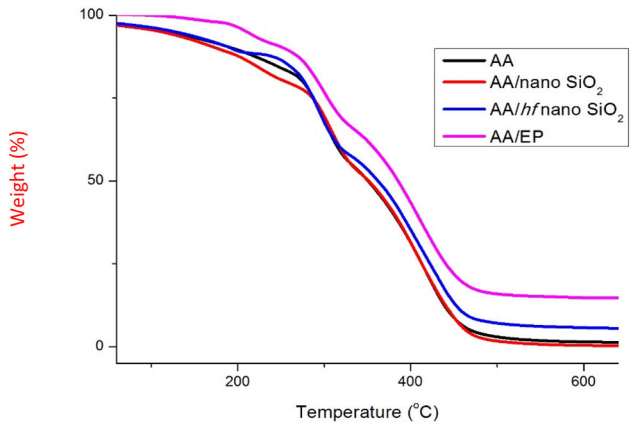

Figure 10. TGA curves of AA and its nanocomposite hydrogels.

Freeze drying, also known as lyophilization, is widely used in the manufacture of porous hydrogels for various applications. This method involves rapidly chilling a system to generate thermodynamic instability and phase separation. The solvent (generally water) is then removed by sublimation under vacuum, leaving voids behind in the areas it occupies.[24] The disadvantage of this approach is that pore creation degrades the hydrogels' mechanical properties, restricting their applicability.

Figure 7 shows the FESEM image of AA hydrogel, which has a completely different morphological character after lyophilization. The 3-dimensional (3 D) network structures, voids and their different stacks are clearly visible.

According to FESEM images of nanocomposite hydrogels after lyophilization (Figure 8), the pore (or void) diameters of the pure AA hydrogel were found to be 4.691 μm on average and pore distributions were not homogeneous. In the FESEM image of nano SiO_2-doped AA nanocomposite hydrogel (Figure 8B), the number of pores increased, and the pore diameter increased to an average of 7.588 μm. In Figure 8C, FESEM image of *hf* nano SiO_2-doped AA nanocomposite hydrogel showed homogeneous-dispersed structure and the pore diameter was found as 8.694 μm, higher than the nano-SiO_2 doped AA nanocomposite hydrogel. In the last image (Figure 8D), the pore diameters of EP-doped AA nanocomposite hydrogel were found 6.464 μm on average and pore distributions were not homogeneous.

All these numerical values are listed in Table 2. Based on these data, the morphological evaluation can be summarized as follows: The number and diameter of pores observed in pure AA hydrogel increased with the effect of added particles. In addition, the compatibility of the matrix and the reinforcing material was found to be superior to the others in *hf* nano SiO_2-doped AA nanocomposite hydrogel with the highest pore diameter and homogeneity.

The distribution of the pores of pure AA and its nanocomposite hydrogels are shown in Figure 9. EDX spectra were taken from the elemental dimension with the mapping

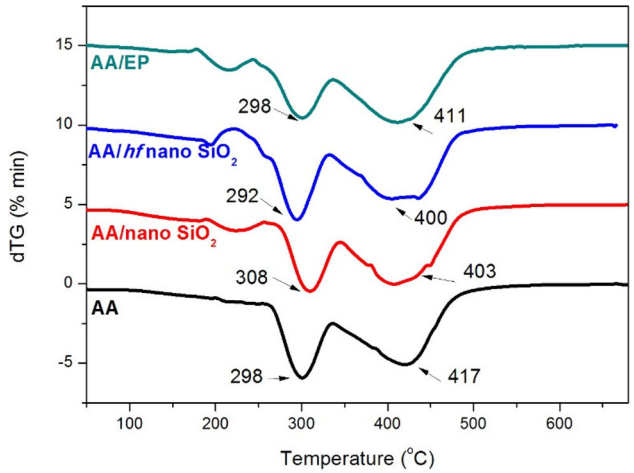

Figure 11. DTG curves of AA and its nanocomposite hydrogels.

method. Although very little amount of SiO_2 which is doped into AA was not observed in EDX, increasing amount of oxygen in mass is the evidence of the presence of SiO_2, as shown clearly in Figure 9B. The element distributions on the maps show that Si and O atoms are present in the structure. In the map of *hf* nano SiO_2-doped AA nanocomposite hydrogel, nitrogen atom is not included in the given elements. Due to the fact that the amount of *hf* nano SiO_2 added to the hydrogel structure is very low and the silanol OH groups replaced with NH_2 groups are much lower levels, no significant results have been obtained regarding the nitrogen atoms in the map evaluation. Finally, Figure 9D indicates that the elements in the expanded perlite were homogeneously distributed across the pores in the hydrogel structure.

The thermal behavior of pure AA and its nanocomposite hydrogels was investigated by TGA/DTG method. According to TGA curves in Figure 10, degradation was mainly occurred in two steps. The loss of mass was observed to be less in nanoparticle-doped state. The EP-doped AA nanocomposite hydrogel indicated the lowest mass loss due to the excess of inorganic elements included. Due to the weak chemical interaction between AA and the small amount of neutral nano SiO_2 added to AA, the thermal decomposition curves were almost observed same. The *hf* nano SiO_2 and EP interacted with AA more intensively than the neutral nano-SiO_2 taking into account mass loss value at the same temperature. The best thermal stability was recorded on EP-doped AA nanocomposite hydrogel. Because EP itself includes many other minerals other than SiO_2. However, since the particle size of EP used in this study is larger than other SiO_2 species, particle and hydrogel compatibility is worse than others. In this way, it is possible to say that the thermal stability as well as the structural stability of *hf* nano SiO_2-doped AA nanocomposite hydrogels are the best.

DTG curves for AA and its nanocomposite hydrogels were given in Figure 11. In literature, the glass transition temperature is recorded as 128 °C for pure PAA. Polymer chains move more conveniently over this temperature.[25] Acrylic acid thermal decomposition curves are divided into two sections. The first disruption was caused by the elimination of side groups in PAA, which led in decarboxylation or anhydride production (approx. 30 percent mass loss at about 300 °C), while the second was caused by main chain scission (approx. 60 percent mass loss at around 410 °C). In the DTG curve of the *hf* nano SiO_2-doped AA nanocomposite hydrogel, the shift of these numerical values to a lower temperature is again a result of the interaction between carboxylate groups of hydrogels and NH_2 groups of *hf* nano SiO_2 via H-bond, as previously mentioned.

Conclusions

During the synthesis conducted as part of the present study, the experimental parameters for all hydrogels were obtained in the same way. The behavior of nano-SiO_2-doped hydrogels was established, and Perlite, a volcanic rock type plentiful in nature and less expensive than nano SiO_2, was doped into acrylic acid hydrogels. Based on the data obtained by observing the pure nano SiO_2 behavior of the nanocomposite hydrogel structure, we were able to learn about the behavior of SiO_2 in perlite. Morphological and structural characterizations were performed by FT-IR and through detailed FESEM analyses. The results revealed that the NH_2-modified nano-SiO_2 was in complete conformity with the AA hydrogels, resulting in improved swelling, morphological and thermal properties. Using the NH_2-modified nano SiO_2 has two advantages. One of them is the electrostatic interaction between the amine groups of the nano-SiO_2 and the carboxylic acid groups of AA. This interaction results in better dispersion of the nano-sized SiO_2 particles in the polymer matrix. Secondly, it has advantages over capturing and adsorption of adsorbates compared to the original AA hydrogel.

The behavior of three different types of SiO_2 reinforcements in composite hydrogels during the planning of a target-focused work with SiO_2-doped nanocomposite hydrogels had significance in the interpretation of the results to be achieved in targeted applications.

Experimental section

Materials

Neutral nano-SiO_2 (15-20 nm, 99.5%, Skyspring nanomaterials), hydrophilic (*hf*) nano-SiO_2 with NH_2 groups via long alkyl chains (10-20 nm, 99.8%, Skyspring nanomaterials), expanded perlite (EP) (ETI Mine Operations), acrylic acid (Sigma-Aldrich), N,N'-methylenebisacrylamide (*N,N'*-MBAAm) as crosslinker (Sigma-Aldrich) and azobisisobutyronitrile (AIBN) as initiator (Merck) were utilized in the forms they were received. Thermo Scientific, Smart2Pure ultra-pure water was used as a solvent in all the procedures.

Most of the materials utilized as a part of the present study have been preferred in consideration of their being environmentally-friendly and ability to work in harmony with the human body. The other reactants such as AIBN and NNMBAAm were used at the lowest amounts in the

reaction (respectively 0.015 g and 0.08 g). Because of the toxicity of the initiator and crosslinking agents, it would be a difficult approach to overcome. Additionally, the exceed of the reactants was tracked by the FT-IR spectrophotometer. All reactants were analyzed individually, and after the polymerization, obtained polymers showed clear spectrums apart from the initiator and crosslinking agent. After having determined the behavior of pure SiO_2 nanoparticles in nanocomposite hydrogels, the volcanic rock type Perlite, which is commonly found in nature and more affordable than the cost of nano SiO_2, was doped to AA hydrogels.

Preparation of hydrogels

The mixture containing monomer (5.5 mol L^{-1}), initiator (0.01 mol L^{-1}), a crosslinking agent (0.05 mol L^{-1}), ultrapure water, and nanoparticles were poured into PVC straws and heated in a temperature-controlled water bath (at 80 °C) for 2 h. The results were optimized by selecting 4 different silica amounts (0.0010 g, 0.0025 g, 0.0050 g, 0.0100 g) for each hydrogel. According to these results, the amount of nano reinforcement with the best distribution was determined as 0.0010 g. All three nano-reinforcing agents were kept constant at the same amount in all experimental parameters. Then, the PVC straws were carefully removed from the bath, cut into cylindrical disks (3-4 mm in length) with a knife, and the hydrogels were dried in air before they were kept in a vacuum oven (35 °C).

Swelling properties

For conversion and swelling assessments, m_o was calculated through Eq. [1] at first for AA hydrogel and nano-SiO_2/NH_2-modified nano-SiO_2/perlite-doped AA nanocomposite hydrogels. After the conversion of monomer into polymer, (%) was calculated by Eq. [2] to determine the crosslinking %, four pieces of dried hydrogels were washed with water and re-dried, and the procedure continued with Eq. [3]. The following equations (Eq. [4]) were used to compute the swelling percentages (S percent) of nanocomposite hydrogels, where m_t represents the mass of swelled hydrogel at time t. m_1 in the equations [1] and [2]: the first weighing of the wet gels after drying; m_1' in eq. [3]: the amount of 3 or 4 identical dried hydrogels; m_2: indicates the number of gels defined by m_1' washed-dried at least 3 times. The "time" indicated by "t" represents the time periods in which the weights of the gels were taken, in hours. The hydrogel reaches its maximum swelling value when it reaches equilibrium.

$$\begin{aligned} &Mass\ of\ [Monomer + Crosslinking + Initiator] = m_o \\ &Mass\ of\ dried\ hydrogels = m_1 \\ &Mass\ of\ 3\ or\ 4\ hydrogels = m_1{}^{1} \\ &Mass\ of\ washed\text{-}dried\ 3\ or\ 4\ hydrogels = m_2 \end{aligned} \quad (1)$$

$$Conversion\ \%\ (C\%):\ \ m_1/m_o * 100 \quad (2)$$

*For calculation of nanocomposite hydrogel's conversion value, the amount of nanoparticles should be substracted from m_1

$$Crosslinking\ \%\ (CL\%) = m_2/(m_1') * 100 \quad (3)$$

$$Swelling\ \%\ (S\%) = [m_t - m_2]/m_{2)} * 100 \quad (4)$$

$$m_t = mass\ of\ swelling\ at\ "t"\ time$$

Instrumental methods

FT-IR analyses were performed on a Perkin Elmer Spectrum 100 model FT-IR in the range 400-4000 cm^{-1}. The ATR mode was employed, and each spectrum was scanned four times and studied at a resolution of 4 cm^{-1}. X-ray powder diffraction patterns of nanocomposite hydrogels were collected using a PANalytical Empyrean X-Ray diffractometer using CuKα radiation (λ1/41.54 Å) in the 2θ range 5°-70° with a scanning speed of 2°/min at room temperature. Field Emission SEM (FESEM) analyses were carried out with a Carl Zeiss Supra 40VP model SEM device. Water-adsorbed hydrogels were placed in a freezer (kept at −18 °C) for 12 h to further analyze the pore architectures of nanocomposite hydrogels, then placed in a vacuum apparatus in frozen states (instrument: Labconco, Freezone 2.5 [Canada] lyophilizer). Hydrogels that had been compressed for 16 h inside the apparatus were studied in FESEM without any deformation due to internal water separation. The hydrogel surfaces were plated with platinum using Quorum brand coating device to ensure conductivity. While the surfaces were being photographed, a SE (secondary detector) was employed. The mapping method was used with the Bruker EDX detector to determine inorganic particle distributions in nanocomposite hydrogels. The same procedure was applied for each sample when preparing samples for SEM analysis. After the "freeze-dry" process, dry gels were cut into equal sizes, the platinum coating was applied under 40 kV for 45 seconds to ensure the conductivity of the surfaces. The coated samples were placed in the SEM device and analyzes were performed with the SE detector at a working distance of about 10 mm and at a working potential of 15 kV. The SETARAM simultaneous TG/DTA equipment was used to conduct TGA analyses. In a N_2 environment, the heating procedure was carried out over a temperature range of 25-690 °C with a heating rate of 10 °C min^{-1}.

Acknowledgement

We are grateful to Bilecik Seyh Edebali University Central Research Laboratory for providing FT-IR, XRD, FESEM and TGA measurements.

ORCID

Fatma Özge Gökmen http://orcid.org/0000-0002-5548-8790
Nursel Pekel Bayramgil http://orcid.org/0000-0001-9925-6361

References

[1] Fisher, O. Z.; Khademhosseini, A.; Langer, R.; Peppas, N. A. Bioinspired Materials for Controlling Stem Cell Fate. *Acc. Chem. Res.* **2010**, *43*, 419–428. DOI: 10.1021/ar900226q.

[2] Kloxin, A. M.; Kloxin, C. J.; Bowman, C. N.; Anseth, K. S. Mechanical Properties of Cellularly Responsive Hydrogels and Their Experimental Determination. *Adv. Mater.* **2010**, *22*, 3484–3494. 2010DOI: 10.1002/adma.200904179.

[3] Slaughter, B. V.; Khurshid, S. S.; Fisher, O. Z.; Khademhosseini, A.; Peppas, N. A. Hydrogels in Repenerative Medicine. *Adv. Mater.* **2009**, *21*, 3307–3329. DOI: 10.1002/adma.200802106.

[4] Gaharwar, A. K.; Peppas, N. A.; Khademhosseini, A. Nanocomposite Hydrogels for Biomedical Applications. *Biotechnol. Bioeng.* **2014**, *111*, 441–453. DOI: 10.1002/bit.25160.

[5] Wichterle, O.; Lim, D. Hydrophilic Gels for Biological Use. *Nature* **1960**, *185*, 117–118. 1960 DOI: 10.1038/185117a0.

[6] Satish, C. S.; Satish, K. P.; Shivakumar, H. G. Hydrogels as Controlled Drug Delivery Systems: Synthesis, Crosslinking, Water and Drug Transport Mechanism. *Ind. J. Pharm. Sci.* **2006**, *68*, 133–140. DOI: 10.4103/0250-474X.25706..

[7] Wang, Q.; Mynar, J. L.; Yoshida, M.; Lee, E.; Lee, M.; Okuro, K.; Kinbara, K.; Aida, T. High-Water-Content Mouldable Hydrogels by Mixing Clay and a Dendritic Molecular Binder. *Nature* **2010**, *463*, 339–343. DOI: 10.1038/nature08693.

[8] Ovando-Medina, V. M.; Reyes-Palacios, G. A.; García-Montejano, L. A.; Antonio-Carmona, I. D.; Martínez-Gutiérrez, H. Electroactive Polyacrylamide/Chitosan/Polypyrrole Hydrogel for Captopril Release Controlled by Electricity. *J. Vinyl Addit. Technol.* **2021**, *27*, 679–690. DOI: 10.1002/vnl.21842.

[9] Hench, L. L.; Polak, J. M. Third-Generation Biomedical Materials. *Science* **2002**, *295*, 1014–1017. DOI: 10.1126/science.1067404.

[10] Gökmen, F. Ö.; Bayramgil, N. P. Synthesis and Characterization of N-[3-(Dimethyl-Amino)Propyl]Methacrylamide/(nano-SiO_2, Amine-Modified nano-SiO_2 and Expanded Perlite) Nanocomposite Hydrogels. *Eur. Chem. Bull.* **2017**, *6*, 514–518. doi:10.17628/ecb.2017.6.514-518.

[11] Peppas, N. A.; Khare, A. R. Preparation, Structure and Diffusional Behavior of Hydrogels in Controlled Release. *Adv. Drug Del. Rev.* **1993**, *11*, 1–35. DOI: 10.1016/0169409X(93)90025-Y.

[12] Anisha, S.; Sharma, P. K.; Garg, V. K.; Garg, G. Hydrogels: A Review. *Int. J. Pharm. Sci. Rev. Res.* **2010**, *4*, 97–105. http://www.globalresearchonline.net/journalcontents/volume4issue2/Article%20016.pdfISSN 0976 – 044X.

[13] Sun, X.; Zhang, G.; Shi, Q.; Tang, B.; Wu, Z. Study on Foaming Water-Swellable EPDM Rubber. *J. Appl. Polym. Sci.* **2002**, *86*, 3712–3717. DOI: 10.1002/app.11381.

[14] Kashyap, N.; Kumar, N.; Ravi Kumar, M. N. V. Hydrogels for Pharmaceutical and Biomedical Applications. *Crit. Rev. Ther. Drug Carrier Syst.* **2005**, *22*, 107–149. DOI: 10.1615/CritRevTherDrugCarrierSyst.v22.i2.10.

[15] Thakur, S.; Arotiba, O. Synthesis, Characterization and Adsorption Studies of an Acrylic Acid-Grafted Sodium Alginate-Based TiO_2 Hydrogel Nanocomposite. *Adsorp. Sci. Technol.* **2018**, *36*, 458–477. DOI: 10.1177/0263617417700636.

[16] Makhado, E.; Pandey, S.; Nomngongo, P. N.; Ramontja, J. Preparation and Characterization of Xanthan Gum-cl-Poly(Acrylic Acid)/o-MWCNTs Hydrogel Nanocomposite as Highly Effective re-Usable Adsorbent for Removal of Methylene Blue from Aqueous Solutions. *J. Colloid Interface Sci.* **2018**, *513*, 700–714. DOI: 10.1016/j.jcis.2017.11.060.

[17] Zhong, C.; He, M.; Lou, K.; Gao, F. The Application Neurotoxicity, and Related Mechanism of Silica Nanoparticles. In *Neurotoxicity of Nanomaterials and Nanomedicine*; Jiang, X., Gao, H., Eds.; Academic Press (Elsevier): United Kingdom, **2017**; pp 227–257. DOI: 10.1016/B978-0-12-804598-5.00010-6.

[18] Murugan, B.; Sagadevan, S.; J, A. L.; Fatimah, I.; Fatema, K. N.; Oh, W.-C.; Mohammad, F.; Johan, M. R. Role of Mesoporous Silica Nanoparticles for the Drug Delivery Applications. *Mater. Res. Express* **2020**, *7*, 102002. ;. DOI: 10.1088/2053-1591/abbf7e.

[19] van den Brom, C. R.; Anac, I.; Roskamp, R. F.; Retsch, M.; Jonas, U.; Menges, B.; Preece, J. A. The Swelling Behaviour of Thermoresponsive Hydrogel/Silicananoparticle Composites. *J. Mater. Chem.* **2010**, *20*, 4827–4839. DOI: 10.1039/b927314j.

[20] Tian, Y.; Tang, Y.; Li, S.; Lv, H.; Liu, P.; Jing, Q. Voigt-Based Swelling Water Model for Super Water Absorbency of Expanded Perlite and Sodium Polyacrylate Resin Composite Materials. *e-Polymers* **2019**, *19*, 365–368. DOI: 10.1515/epoly-2019-0038.

[21] Pourjavadi, A.; Tehrani, Z. M.; Salimi, H.; Banazadeh, A.; Abedini, N. Hydrogel Nanocomposite Based on Chitosan-g-Acrylic Acid and Modified Nanosilica with High Adsorption Capacity for Heavy Metal İon Removal. *Iran Polym. J.* **2015**, *24*, 725–734. DOI: 10.1007/s13726-015-0360-1.

[22] Kabra, S.; Katara, S.; Rani, A. Characterization and Study of Turkish Perlite. *Int. J. Innov. Res. Sci. Eng. Technol.* **2007**, *2*, 4319–4326.

[23] Vetriselvi, V.; Jaya Santhi, R. R. Synthesis and Characterization of Poly Acrylic Acid Modified with Dihydroxy Benzene-Redox Polymer. *Res. J. Chem. Sci.* **2014**, *4*, 1–9.

[24] Annabi, N.; Nichol, J. W.; Zhong, X.; Ji, C.; Koshy, S.; Khademhosseini, A.; Dehghani, F. Controlling the Porosity and Microarchitecture of Hydrogels for Tissue Engineering. *Tissue Eng. Part B Rev.* **2010**, *16*, 371–383. DOI: 10.1089/ten.TEB.2009.0639.

[25] Dubinsky, S.; Grader, G. S.; Shter, G. E.; Silverstein, M. S. Thermal Degradation of Poly(Acrylic Acid) Containing Copper Nitrate. *Polym. Degrad. Stab.* **2004**, *86*, 171–178. DOI: 10.1016/j.polymdegradstab.2004.04.009.